# A Comparison of FDTD-Predicted Surface Magnetic Fields with SuperMAG, INTERMAGNET, and SWMF/RIM Virtual Magnetometers during a Geomagnetic Storm

Yisong Zhang[1], Jamesina J Simpson[1], Aaron J Ridley[2], Daniel T Welling[3] and Michael Warren Liemohn[4]

[1] University of Utah, Salt Lake City, UT, United States, [2] University of Michigan, Ann Arbor, MI, United States, [3] University of Texas at Arlington, Arlington, TX, United States, [4] University of Michigan, Climate and Space Sciences and Engineering, Ann Arbor, MI, United States

#### PRESENTED AT:



#### INTRODUCTION

The historical record indicates the possibility of intense coronal mass ejections (CMEs). Energized particles and magnetic fields ejected by coronal mass ejections (CMEs) towards the Earth may disrupt the Earth's magnetosphere and generate a geomagnetic storm. During a geomagnetic storm, the induced geoelectric field can drive geomagnetically-induced currents (GICs) that ow through ground-based conductors. These GICs have the potential to damage high voltage power transmission systems and cause blackouts.

As part of the NSF-funded Comprehensive Hazard Analysis for Resilience to Geomagnetic Extreme Disturbances (CHARGED) project, a solar-wind-to-lithosphere numerical model of the geoelectric field is being developed. The purpose of this new tool is to drive a new generation of GIC forecasting. As a part of that work, Maxwell's equations, finite-difference time-domain (FDTD) models of the last stage of the Sun-to-Earth propagation path is being coupled to output generated by the Block Adaptive Tree Solarwind Roe-type Upwind Scheme (BATS-R-US) magnetohydrodynamics model and the Ridley Ionosphere Model (RIM) of ionospheric dynamics.

Specifically, three-dimensional (3-D) Space Weather Modeling Framework(SWMF)/Ridley Ionosphere Model (RIM)-predicted ionospheric currents occurring in the lower ionosphere during and around the time of the March 17, 2015 storm are modeled in 3-D FDTD models of North America. The FDTD-calculated results are compared with surface magnetic fields measured in the region by SuperMAG and INTERMAGNET magnetometers. The FDTD results are also compared with virtual magnetometer data (Gannon et al., 2019), which calculates the perturbation of the surface magnetic field using output from the SWMF/RIM magnetohydrodynamics model.

# **INPUT DATA**

A vertical diagram of the 3D FDTD model is shown in Figure 3. The bottom portion of the grid modules the ground and oceans. Free space is assumed from ground level to an altitude of 100 km. From 100 km to 145 km, ionosphere currents from SWMF/RIM are assigned. The top layer of these currents (145 km) is extended upward to the upper Perfect Electrical Conductor (PEC) boundary of the grid at 635 km. The PEC on the top side of the grid mirrors the ionospheric currents below it to create a complete current loop.

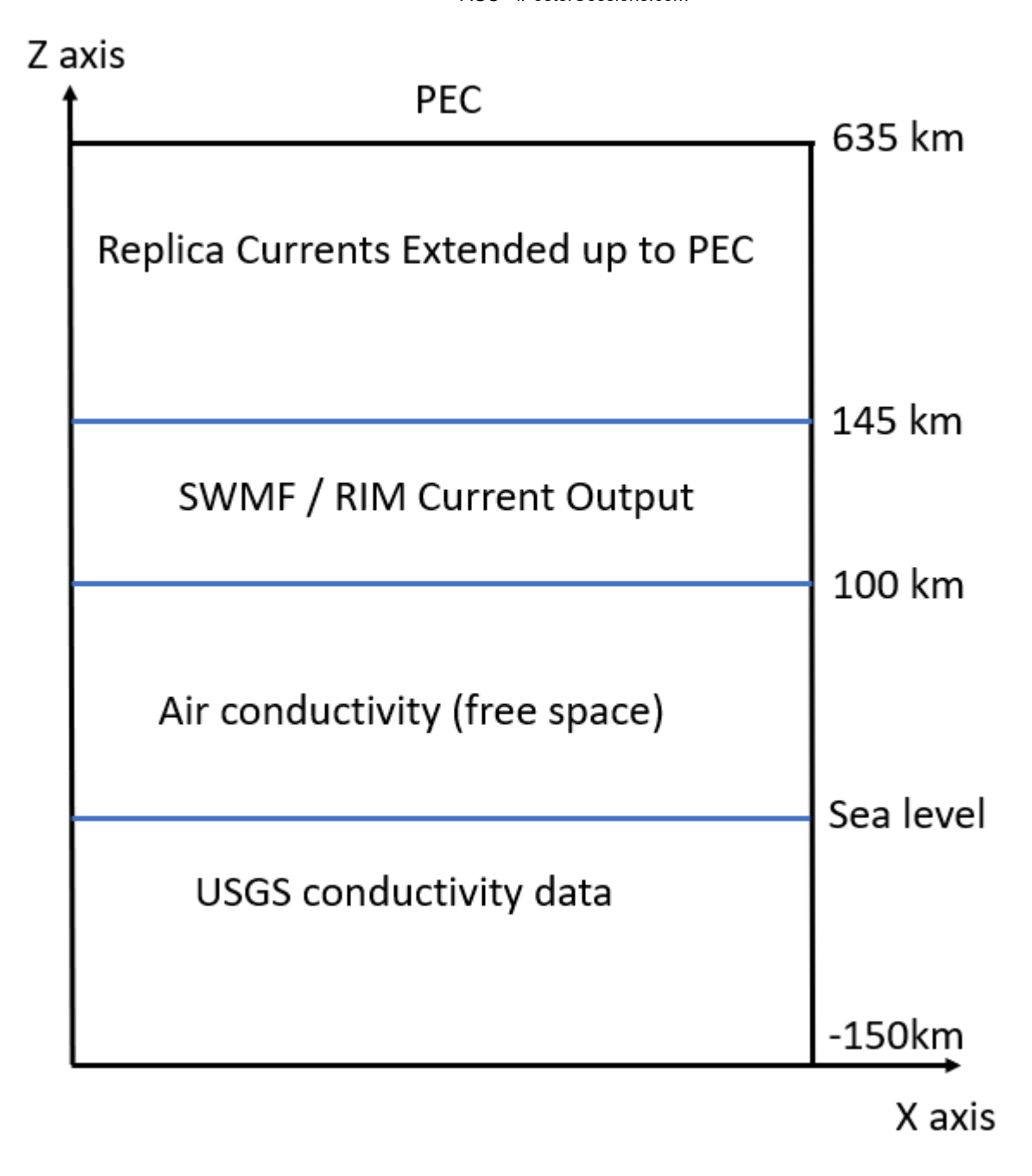


Figure 3. Model distribution on the vertical direction (Note: not drawn to scale)

Using the Earth's topography (NOAA-NGDC), ground and ocean electrical conductivity values are assigned, as shown in Figure 4. 3D Earth conductivities from the United States Geological Survey (USGS) are used for the region covering the U.S. (Kelbert et al., 2009; Semenov & Kuvshinov, 2012; Sun et al., 2015). The northernmost U.S. ground conductivity values are extended to the north and used as the conductivity values in southern Canada. This is because detailed 3D ground conductivity data is not available yet for Canada.

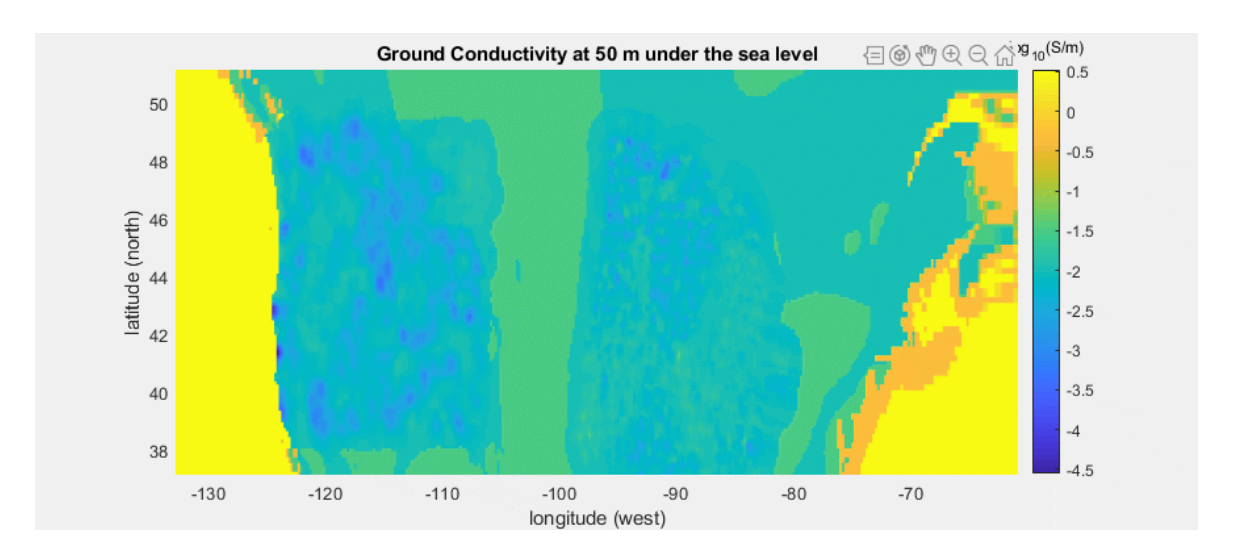


Figure 4. Animation of the 3D ground conductivities at different depths (Kelbert et al., 2009; Semenov & Kuvshinov, 2012; Sun et al., 2015)

Ionosphere currents from the Space Weather Modeling Framework (SWMF) / Ridley Ionosphere Model (RIM) are used as a source in Maxwell's equations FDTD model. Only the Pederson and Hall currents from SWMF/RIM are modeled. Figure 5 shows the time evolution of the input ionospheric currents at an altitude of 115 km over time.

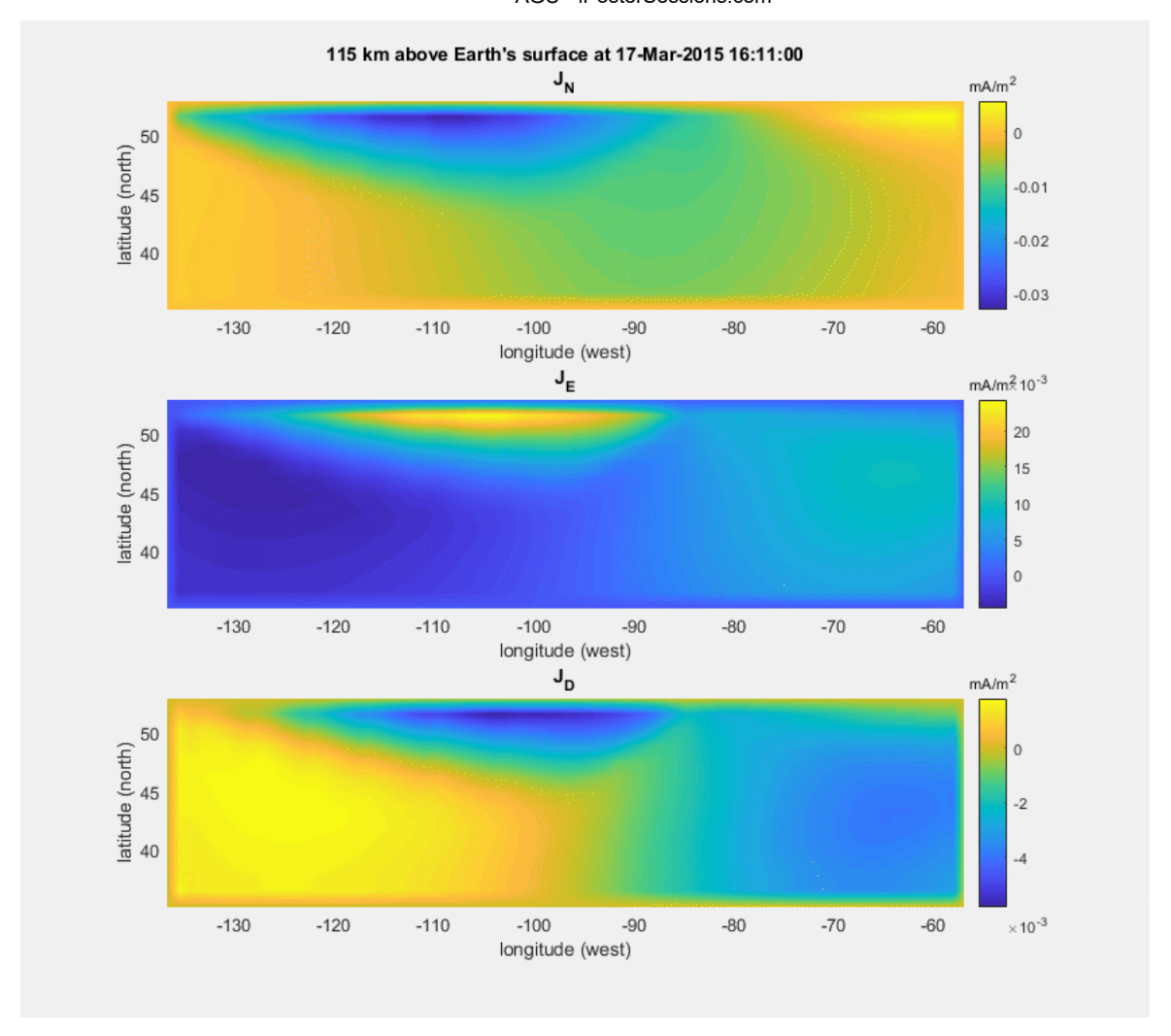


Figure 5. SWFM/RIM output current at 115 km

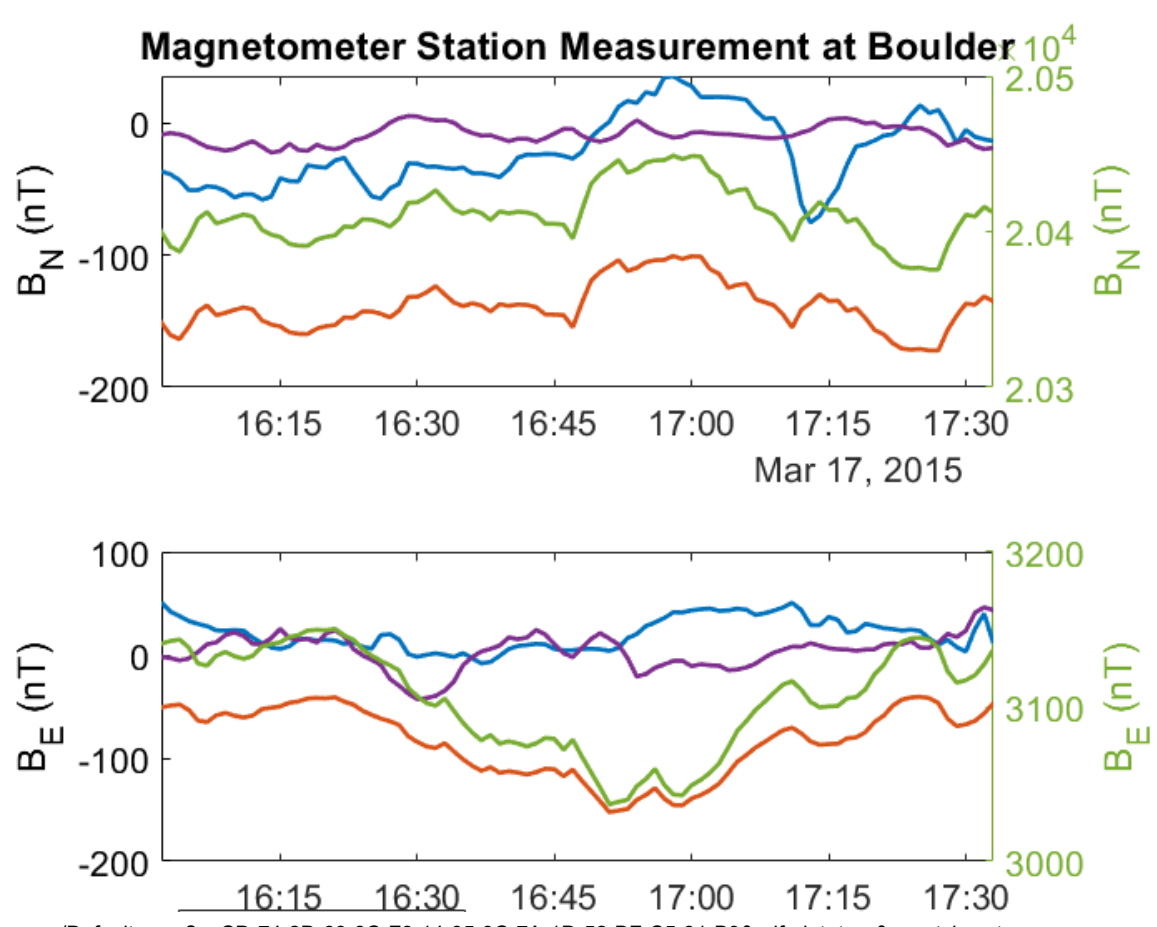
### **RESULTS AND DISCUSSION**

The animation in the middle image gallery shows the behavior of the FDTD-calculated surface magnetic fields as well as the SWMF/RIM ionospheric currents occurring at 115 km over 1 hour and 44 minutes, and at a resolution of 1 minute. The coordinate system defines N as geographic north, E as geographic east, and D as down.

Notice in the animation that there is a correlation between the B\_N and J\_E components, as well as the B\_E and J\_N components. Also, the effect of the ocean-continent boundaries is visible in the surface B fields.

Next, the magnetic field at the Earth's surface is recorded in the FDTD model at Boulder, CO over the 1 hour and 44 minutes. Both  $\Delta B$  and dB/dt are shown in Figures 6 and 7.

The results in Figures 6 and 7 indicate that both the magnetic field and dB/dt results from the FDTD model show similar characteristics as the measured data and the SWMF/RIM predicted results.



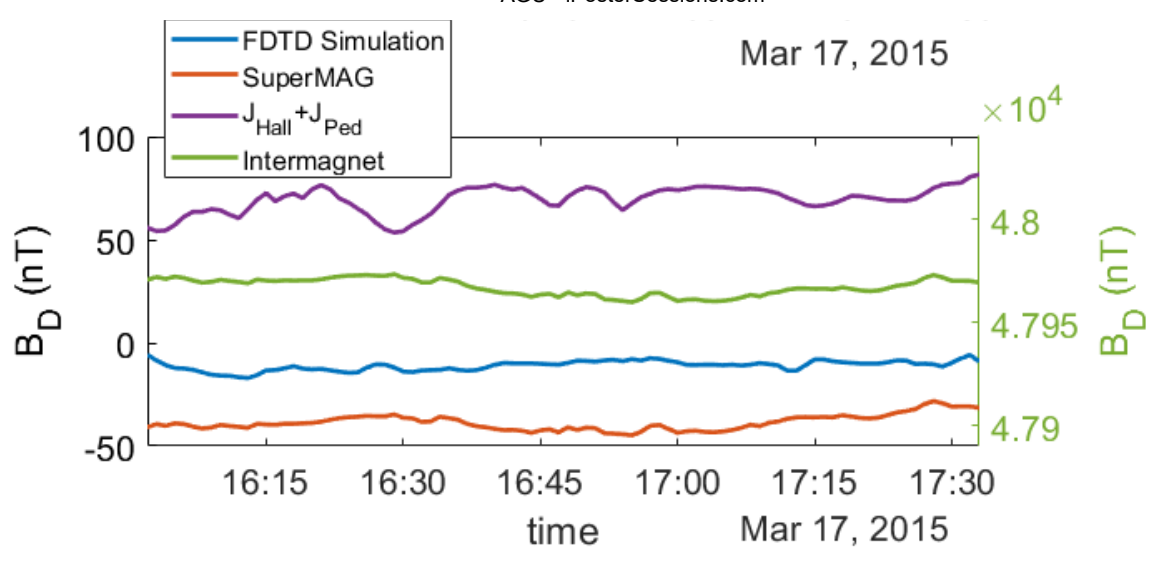
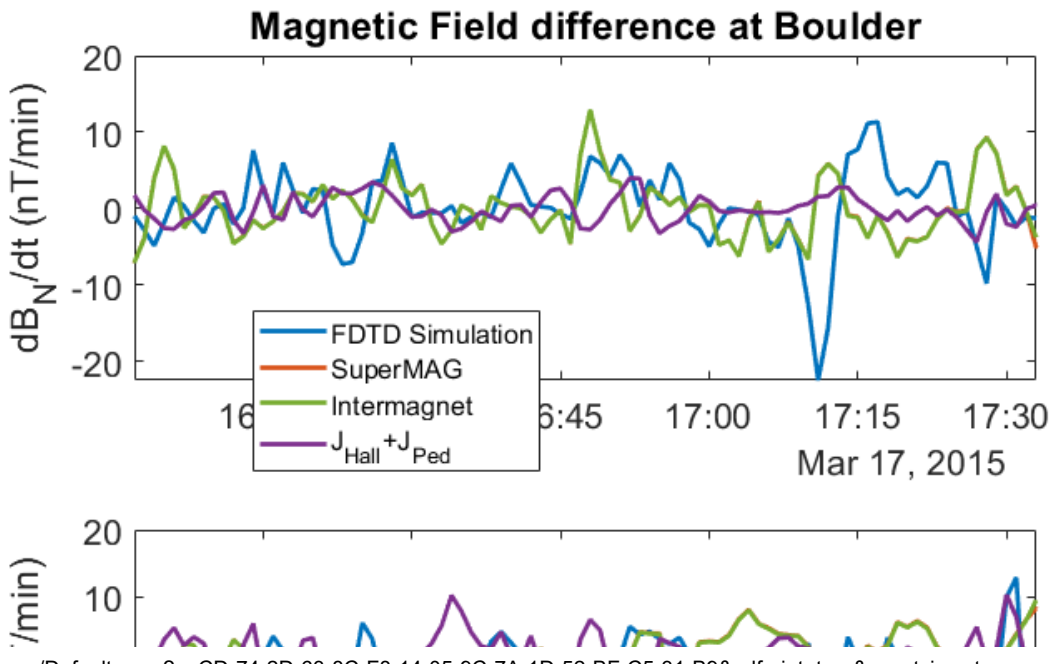


Figure 6. The magnetic field from FDTD, Intermagnet, SuperMAG, and the SWMF/RIM virtual magnetometer. The right y-axis corresponds to the Intermagnet data. The left y-axis corresponds to the other three curves. (Note: In the legend, " $J_{Hall} + J_{Ped}$ " corresponds to the SWMF/RIM virtual magnetometer data)



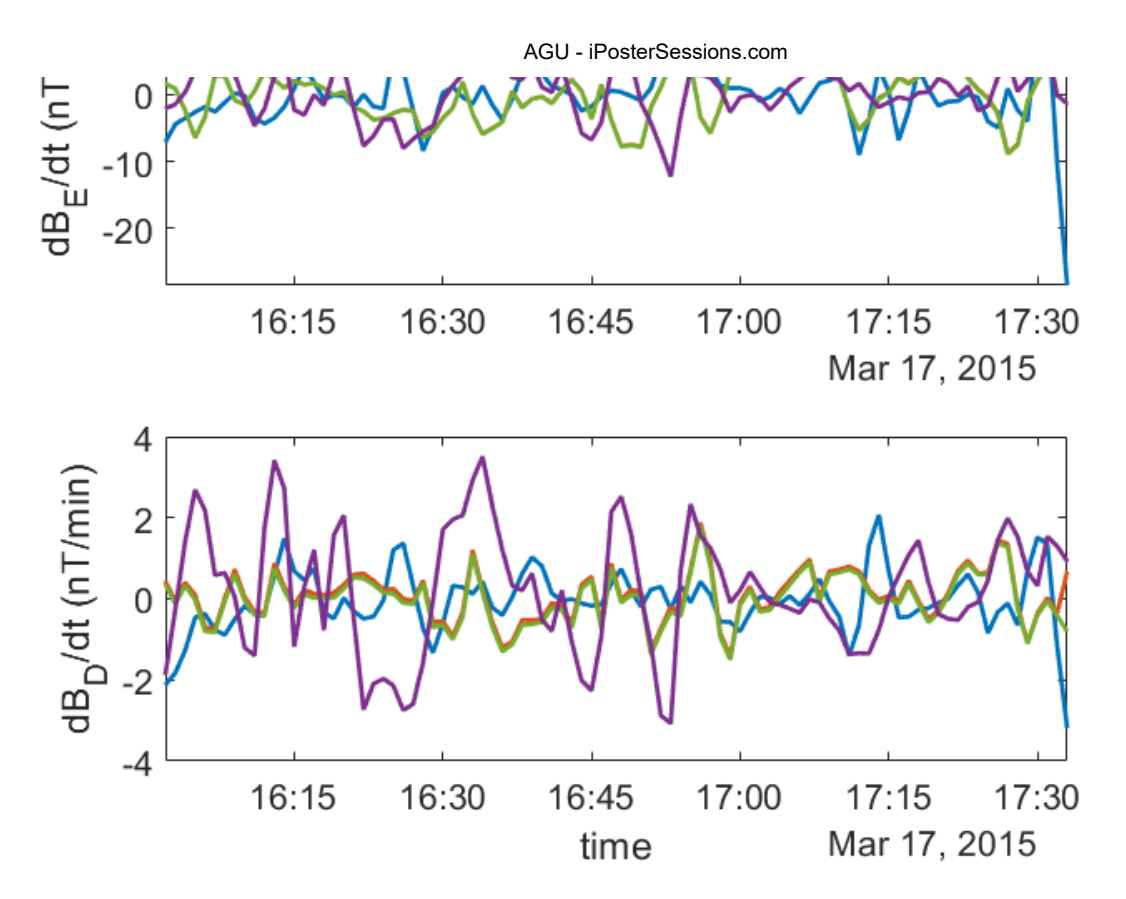


Figure 7. The dB/dt curves from FDTD, Intermagnet, SuperMAG, and the SWMF/RIM virtual magnetometer.

# FUTURE WORK: GLOBAL FDTD MODEL

The periodic boundary conditions (PBCs) implemented in the FDTD model allow us to run a relatively small simulation in a reasonable amount of time. However, the PBCs are non-physical. Therefore, the results in the animation in the middle image gallery are most realistic in the center of the grid rather than the horizontal edges.

As a result, as the next step, we will be running analogous using a global FDTD model. The global FDTD module will account for all of the SWMF/RIM.

# METHOD: FDTD MODEL

The finite-different time-domain (FDTD) method solves Maxwell's equations over a 3-D spatial grid. Each cell of the 3D grid has electric and magnetic field components that are staggered in space as shown in Figure 1. All six electric and magnetic field components are updated in time and space using central differencing.

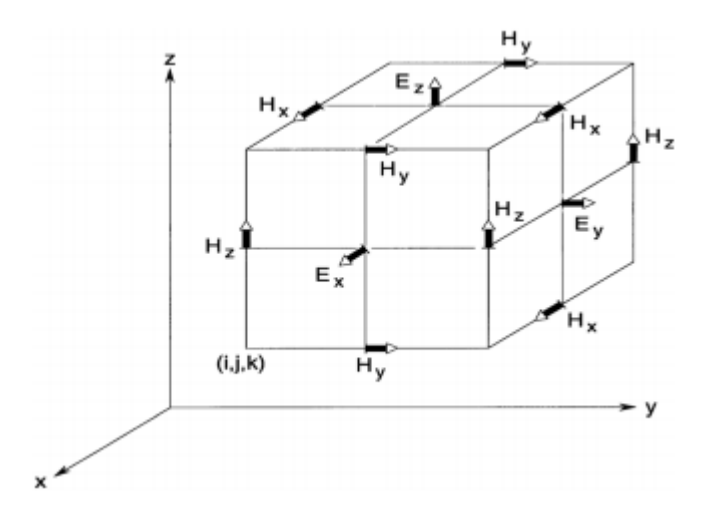


Figure 1. One grid cell of the 3D FDTD model (Yee, 1966)

For this project, the FDTD model extends over the northern U.S. and southern Canada, as shown in Figure 2. In the radial directions, the model extends from 150 km below sea level to an altitude of 635 km. The resolution of the FDTD model is 22 km (East-West) x 11 km (North-South) x 5 km (radially).



Figure 2. The FDTD model's horizontal range  $(37.15^{\circ}N - 51.05^{\circ}N, 132.75^{\circ}W - 60.95^{\circ}W)$ 

#### **Boundary Conditions:**

The lower boundary of the model is 150 km underground. A Surface Impedance Boundary Condition (SIBC) (Taflove & Hagness, 2005) is used to approximate the ground as an infinite medium.

A Perfect Electrical Conductor (PEC) boundary condition is used for the upper boundary. This PEC boundary is used to mirror the lower ionospheric currents (from 100 km to 635 km) in order to create a complete current loop. This ensures the continuity of currents.

Along the horizontal edges of the model, a periodic boundary condition (PBC) is implemented to connect the east and west sides of the grid, and also the north and south sides of the grid. These PBCs are implemented in a manner to ensure continuity of current. The PBCs also approximate the continuation of the earth ionosphere waveguide in the horizontal directions.

#### **ACKNOWLEDGE**

Computational and Information Systems Laboratory. 2019. Cheyenne: HPE/SGI ICE XA System (University Community Computing). Boulder, CO: National Center for Atmospheric Research. doi:10.5065/D6RX99HX.

The support and resources from the Center for High Performance Computing at the University of Utah are gratefully acknowledged.

This material is based upon work supported by the National Science Foundation under Grant No. 1662318.

The results presented in this paper rely on data collected at magnetic observatories. We thank the national institutes that support them and INTERMAGNET for promoting high standards of magnetic observatory practice

For the ground magnetometer data we gratefully acknowledge: Intermagnet; USGS, Alan Thomson; CARISMA, PI Ian Mann; CANMOS, Geomagnetism Unit of the Geological Survey of Canada; The S-RAMP Database, PI K. Yumoto and Dr. K. Shiokawa; The SPIDR database; AARI, PI Oleg Troshichev; The MACCS program, PI M. Engebretson; GIMA; MEASURE, UCLA IGPP and Florida Institute of Technology; SAMBA, PI Eftyhia Zesta; 210 Chain, PI K. Yumoto; SAMNET, PI Farideh Honary; IMAGE, PI Liisa Juusola; Finnish Meteorological Institute, PI Liisa Juusola; Sodankylä Geophysical Observatory, PI Tero Raita; UiT the Arctic University of Norway, Tromsø Geophysical Observatory, PI Magnar G. Johnsen; GFZ German Research Centre For Geosciences, PI Jürgen Matzka; Institute of Geophysics, Polish Academy of Sciences, PI Anne Neska and Jan Reda; Polar Geophysical Institute, Alexander Yahnin and Yarolav Sakharov; Geological Survey of Sweden, Gerhard Schwarz; Swedish Institute of Space Physics, Masatoshi Yamauchi; AUTUMN, PI Martin Connors; DTU Space, Thom Edwards and PI Anna Willer; South Pole and McMurdo Magnetometer, PI's Louis J. Lanzarotti and Alan T. Weatherwax; ICESTAR; RAPIDMAG; British Artarctic Survey; McMac, PI Dr. Peter Chi; BGS, PI Dr. Susan Macmillan; Pushkov Institute of Terrestrial Magnetism, Ionosphere and Radio Wave Propagation (IZMIRAN); MFGI, PI B. Heilig; IGFPAS, PI J. Reda; University of L'Aquila, PI M. Vellante; BCMT, V. Lesur and A. Chambodut; Data obtained in cooperation with Geoscience Australia, PI Marina Costelloe; AALPIP, co-PIs Bob Clauer and

Michael Hartinger; SuperMAG, PI Jesper W. Gjerloev; Data obtained in cooperation with the Australian Bureau of Meteorology, PI Richard Marshall.

#### **ABSTRACT**

The historical record indicates the possibility of intense coronal mass ejections (CMEs). Energized particles and magnetic fields ejected by coronal mass ejections (CMEs) towards the Earth may disrupt the Earth's magnetosphere and generate a geomagnetic storm. During a geomagnetic storm, the induced geoelectric field can drive geomagnetically-induced currents (GICs) that flow through ground-based conductors. These GICs have the potential to damage high voltage power transmission systems and cause blackouts.

As part of the NSF-funded Comprehensive Hazard Analysis for Resilience to Geomagnetic Extreme Disturbances (CHARGED) project, a solar-wind-to-lithosphere numerical model of the geoelectric field is being developed. The purpose of this new tool is to drive a new generation of GIC forecasting. As a part of that work, Maxwell's equations, finite-difference time-domain (FDTD) models of the last stage of the Sun-to-Earth propagation path is being coupled to output generated by the Block Adaptive Tree Solarwind Roe-type Upwind Scheme (BATS-R-US) magnetohydrodynamics model and the Ridley Ionosphere Model (RIM) of ionospheric dynamics.

Specifically, three-dimensional (3-D) BATS-R-US and RIM-predicted ionospheric currents occurring in the lower ionosphere during and around the time of the March 17, 2015 storm are modeled in 3-D FDTD models of North America. These models start at a depth of 150 km, and they account for ionospheric currents occurring up to an altitude of 115 km. The resolution of the FDTD models is 22 km (East-West) x 11 km (North-South) x 5 km (radially), and they account for 3-D lithosphere conductivities provided by the U.S. Geological Survey.

The FDTD-calculated results are compared with surface magnetic fields measured in the region by SuperMAG and INTERMAGNET magnetometers. The FDTD results are also compared with virtual magnetometer data, which calculates the perturbation of the surface magnetic eld using output from the BATS-R-US magnetohydrodynamics model. Comparison plots and an analysis of the results will be provided.

#### **REFERENCES**

Yee, K. S. (1966). Numerical solution of initial boundary value problems involving Maxwell's equations in isotropic media. IEEE Transactions on Antennas and Propagation, 14, 302–307.

Gannon, J., A. Swidinsky, and Z. Xu (2019), Geomagnetically induced currents from the sun to the power grid, 1st ed., John Wiley & Sons, Inc.

Viljanen, A., H. Nevanlinna, K. Pajunpa"a, and A. Pulkkinen, 2001. Time derivative of the horizontal geomagnetic field as an activity indicator. Annales Geophysicae, 19(9), 1107–1118. 10.5194/angeo-19-1107-2001.1

Pokhrel, S., V. Shankar, and J. Simpson (2018), 3-D FDTD Modeling of Electromagnetic Wave Propagation in Magnetized Plasma Requiring Singular Updates to the Current Density Equation, IEEE Transactions on Antennas and Propagation, 66(9), 4772-4781.

Taflove, A., & Hagness, S. C. (2005). Computational electrodynamics: The finite-difference time-domain method (3rd ed.). Norwood, MA: Artech House.

Kelbert, A., Schultz, A., & Egbert, G. (2009). Global electromagnetic induction constraints on transition-zone water content variations. Nature, 460(7258), 1003–1006. http://doi.org/10.1038/nature08257

Semenov, A., & Kuvshinov, A. (2012). Global 3-D imaging of mantle conductivity based on inversion of observatory C responses-II. Data analysis and results. Geophysical Journal International, 191(3), no-no. http://doi.org/10.1111/j.1365-246X.2012.05665.x

Sun, J., Kelbert, A., & Egbert, G. D. (2015). Ionospheric current source modeling and global geomagnetic induction using ground geomagnetic observatory data. Journal of Geophysical Research: Solid Earth, 120(10), 6771–6796. http://doi.org/10.1002/2015JB012063

National Oceanic and Atmospheric Administration(NOAA) - National Geophysical Data Center (NGDC), Global Relief CD-ROM